Expertise
and insight
for the future

Sean Haslam

Electric Sail and Plasma Brake Deployment System Prototype

Metropolia University of Applied Sciences

Bachelor of Engineering

Electronics

Thesis

13th November 2018

Author	Sean Haslam
Title	Electric Sail and Plasma Brake Deployment System Prototype
Number of Pages	33 pages
Date	13th November 2018
Degree	Bachelor of Engineering
Degree Programme	Electronics
Professional Major	
Instructors	Jouni Envall, Research Scientist Anssi Ikonen, Senior Lecturer

This thesis will detail the prototyping and results of the main and peripheral functions of a deployment system for electric sail and plasma brake technologies. The aim of this project is to provide a fully functioning prototype that may be developed further into engineering qualification models, and finally culminating in a flight model.

First the thesis will clarify cubesat technology, the science of these technologies, followed by covering the schematic and subsystems for the deployment system. The study utilises some FORESAIL-1 mission specifications as a basis for development.

The prototype was implemented using standard retail components and a STM32 microcontroller embedded on an evaluation board. Programming of the STM32 was accomplished with Keil integrated development environment using C language. Command communication, for simulation of the commands an On-Board Computer would send to payloads, is achieved with YAT Terminal and a universal asynchronous receiver-transmitter interface. Measurements were executed with a digital multimeter, oscilloscope and the STM32s built-in analog-to-digital converters.

For the results, the functionality of the prototype is analysed and assessed. The results are compared with the calculations. Finally this report will discuss the improvements that can be applied for future iterations.

Keywords	Electric Sail, Plasma Brake, Deployment, Cubesat, Flatsat, Prototype, FORESAIL-1, ESTcube-2

Contents

List of Abbreviations

EQM	Engineering qualification model. Prototype consisting of both flight-grade and commercial components.
FM	Flight Model. A fully functional model that has undergone rigorous inspection and testing. This model is the final iteration, and is ready for launch.
IC	Integrated circuit. Made typically of silicon wafers and may contain millions upon millions of transistors, but also resistors, diodes, capacitors among other components.
MCU	Microcontroller Unit. A CPU with integrated peripherals, such as memory, RAM, and general purpose inputs and outputs.
OBC	On-Board Computer. Main computer aboard a satellite for controlling systems and communication.
PCB	Printed circuit board. A mechanical structure onto which electronic components are soldered and electrically connected.
NASA	National Aeronautics and Space Administration. United States government organization, also devoted to space exploration.
MOSFET	Metal-Oxide-Semiconductor Field Effect Transistor. A voltage controlled transistor.
CMOS	Complimentary Metal-Oxide-Semiconductor. Integrated circuit logic family composed of complimentary pairs of n-type and p-type MOSFETS
TTL	Transistor-transistor logic. Integrated circuit logic family consisting of bipolar junction transistors.
LEO	Low Earth orbit. An orbit of less than 2000km above the Earth's surface.

1 Introduction

The electric sail and plasma brake are extremely versatile inventions by Pekka Janhunen of the Finnish Meteorological Institute. They are experimental space propulsion devices that generate thrust via the coulomb drag phenomena. By extending a long thin tether into space and charging it to a high positive or negative electric potential, thrust can be produced by the interaction of solar wind particles with the electric field created by the tether. It is primarily aimed at providing propellantless propulsion for space travel in the solar system, which is the function of the electric sail. Furthermore, this technology implemented with minor changes creates a plasma brake, which allows for deorbiting of satellites within a planet's magnetic field. This technology is already implemented as a payload for a technological demonstration experiment on Aalto-1 and ESTcube-1 and will be implemented on future microsatellite missions. Missions planned will include FORESAIL-1/2/3 and ESTcube-2. These missions will be investigating the application of both the electric sail and plasma brake, their viability and improving the Technological Readiness Level of said technologies.

The motivation for creating and implementing this technology is many-fold. It could significantly reduce the weight and cost of spacecraft and allow easy access to study the outer and inner solar system. The technology is also suited for Earth orbiting satellites, as the plasma brake is perfect for removing satellites from orbit at the end of their lifecycle. With the plasma brake, spacecraft attitude can be actively reduced leading to disintegration on atmospheric re-entry. This removes large fragments of fast traveling space junk from potentially colliding with other satellites or spacecraft. The main aim of this study is to provide a functioning prototype that serves as a basis for developing the EQM.

2 Technologies

2.1 Cubesat

The cubesat standard was initially conceived between Stanford University and California Polytechnic State University in 1999. Created with the goal of providing easy access to space for the purpose of research and experiments by universities and students, it details

specific standards for cubesat designs and payloads that reduce costs and complexity of satellite design significantly.

Microsatellites are classed by weight, with cubesats typically weighing anywhere between 1 kilogram to 10 kilograms. Often, they are built from basic commercial components, but may include flight-rated components too. This platform is ideal for allowing access to space for experimentation by universities and institutes that lack the funding that European Space Agency or NASA possess. For this reason, cubesats are a perfect platform for carrying out the experiments essential to proving the applicability of the electric sail and plasma brake technologies

Cubesats are made up of units, where each unit is standardized as a 10cm by 10cm by 10cm cube, or one litre by volume. A cubesat may range from a 1 unit cubesat to up to 6 units, as specified by the standard. These satellites typically carry a central OBC (On-Board Computer), which controls communication, navigation, data storage, among other functions dependent on the mission and payloads. A payload typically takes one unit of space. All mechanical and electrical designs of payloads, such as OBC or electric sail designs must conform to this standard. [1]

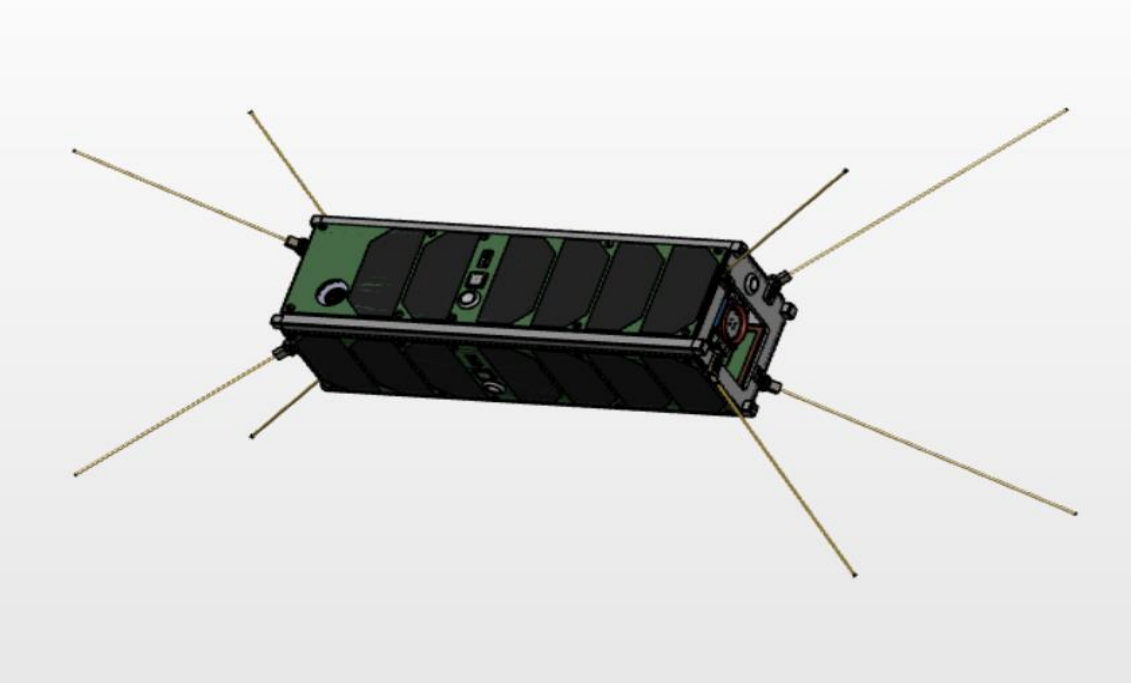

Figure 1. Foresail-1 mechanical design. Provided by Arno Alho of Aalto University (no source available).

Figure 1 illustrates a typical design for a 3 unit (3U) cubesat. In this case, FORESAIL-1, which carries two payloads as well as the central unit. A total of eight antennas extend outward from both ends, typically for communication in VHF/UHF or S-band frequency with the ground station. The surface is covered with solar panels, which are used to provide system power and charge the lithium ion batteries. Within the central unit is housed the OBC, which handles many vital tasks necessary for a successful mission. Such tasks may include attitude determination and navigation, communication with the ground segment and between OBC and payloads. Depending on mission specifications, the OBC may also handle data storage.

2.2 Electric Sail

The electric sail is rather simple in design and implementation. It receives momentum from the constant stream of extremely energetic charged particles emanating from the Sun. This particle stream is known as solar wind. The solar wind consists of a balanced quantity of negatively and positively charged particles, mostly protons and electrons. These particles are ejected outward at high energy in all directions from the Sun at an average speed of 400km/s. By extending metallic and conductive electrostatic tethers into the stellar medium, and charging them to a positive high electric potential, we may interact with the charged particles within the solar wind. The aim is to use protons and positive ions within the solar wind, as their mass is several magnitudes larger than that of electrons, which results in more force transmitted. It is worth mentioning that the mass of protons is magnitudes larger than an electron, thus protons are capable of delivering more newtons of thrust force than electrons.

When a tether is charged to a high voltage in the magnitude of 10^4 volts, it generates a large static electric field around the spacecraft and tether. When positively charged particles travel within this electric potential, they will be deflected away from the electric field, thus imparting their momentum. Electrons will however be attracted to the electric field and will conduct along the tethers to the spacecraft chassis. In order to maintain the large voltage across the tether, these excess electrons must be expelled from the spacecraft. This can be achieved with an electron gun. The main limitation that exists for the electric sail, is the inability to function outside the heliosphere or within a magnetosphere as there is no solar wind. Like a sailboat, an electric sail may be inclined to generate thrust in any

direction, even against the direction of the solar wind by using the traditional tacking method as used by sailors for sailing against the wind on Earth.

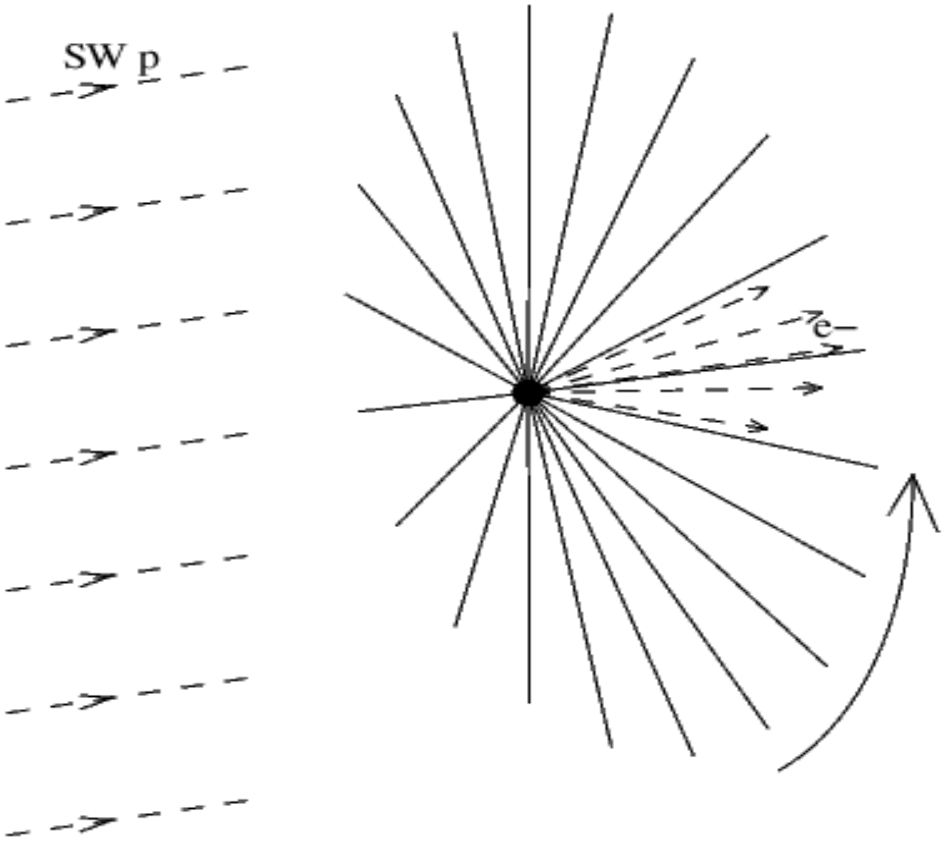

Figure 2. Sketch of core concept and design of an electric sail. Reprinted from [2,2]

In the above figure 2, we can see the basic concepts describing the electric sail function using multiple tethers. The spacecraft is set spinning during deployment, so that centrifugal force can be used to keep the tethers straight. The tethers are then charged to a high positive potential, creating a strong electric field with a large effective area around the spacecraft. Excess electrons will be accumulated within the tethers and conducted to the electron gun, which shoots them away from the spacecraft so that the positive potential on the tether is maintained. [2.]

Electric sail also serves as a novel instrument for measuring micrometeoroid flux and plasma densities in the stellar medium or around celestial bodies. Micrometeoroids are

detected by monitoring voltage transients in the tether, caused by micrometeoroids impacting the tether. Plasma density is then measured by determining the current travelling through the tether. This helps us understand the space weather and hazards around celestial bodies, such as the Moon or Earth better.

2.3 Plasma Brake

This essentially a reverse polarity operation of the electric sail, which lends more versatility to this electric propulsion technology. By charging the tethers to a negative voltage, as seen from satellite chassis, in the magnitude of 10^3 volts, the behaviour of the tether when interacting with charged particles in the presence of a magnetosphere changes drastically. In this situation the tether interacts with the plasma ram flow within a magnetosphere to generate braking thrust towards the gravity gradient of a celestial body.

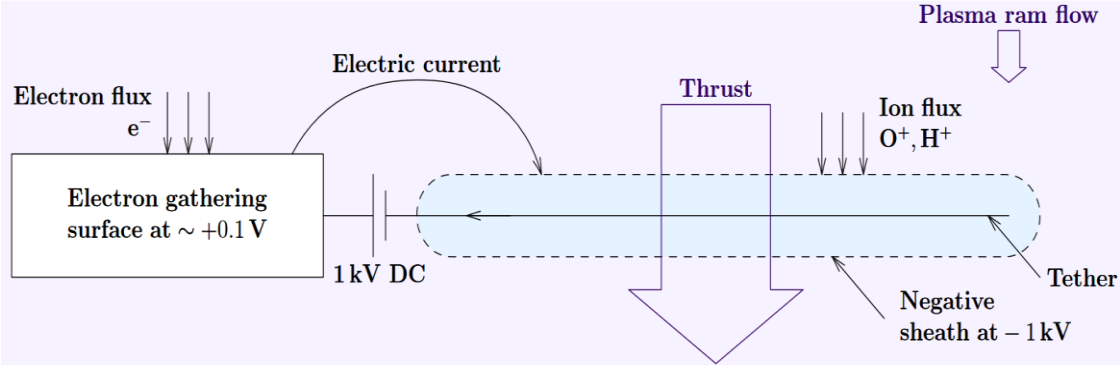

Figure 3. Plasma brake interaction with Earth orbit environment. [3, 8]

In the above figure 3, the plasma brake system and satellite interaction with energized ions and electrons in the surrounding environment is seen. The tether is charged to negative 1kV. Electrons are drawn in to the surface of the satellite, while oxygen and hydrogen ions are drawn in towards the tether creating the plasma ram flow. [3.]

2.4 Tether and Deployment

Tether dimensions for a functional and practical electric sail requires a length of twenty to fifty kilometres, with a thickness of 25 microns, thinner than a human hair. The length

of the tether and strength of the electric field allow it to have a large effective area that extends beyond the tethers. It is designed for electrostatic operation and possesses a redundant mechanical structure for persevering against the constant dangers that micro-meteoroids and other tiny space debris pose. The tether will also have a small mass attached to the tip to aid in deployment. This tip along with the tether reel will have to be secured in place with a locking mechanism.

With the plasma brake a similar tether thickness of 25 microns is desired, but the required length is smaller. For example, FORESAIL-1 aims to deorbit a cube satellite from 800 kilometre orbit to a 600 kilometre orbit using only a 300 metre tether.

Deployment is however the most difficult aspect of this technology's application. Deploying such a long and fragile wire in a low or zero gravity gradient is difficult as the tether has no inclination to stay straight. These issues may be possible to circumvent for short tether wires. By bringing the satellite to a spin of about 180deg/sec, it is possible to create a centrifugal force acting on the tether tip's mass. This will keep the tethers stretched out straight, thus avoiding tangling issues with itself and the satellite. However, the centrifugal force decays logarithmically as the tethers length from the reel to the tip increases, leading to possible tangling and other unwanted behaviour. There is also the danger of the tether simply snapping away during or even after deployment.

3 System Prototype

This section will discuss the prototype and its subsystems, including an overview of the entire system. A description of the MCU involved and how it is setup, along with a short description of the electrical interfacing and communication protocol will be given. Various subsystems and components necessary for executing a functional prototype will also be discussed. Initial calculations necessary for correct functioning of the prototype are also covered.

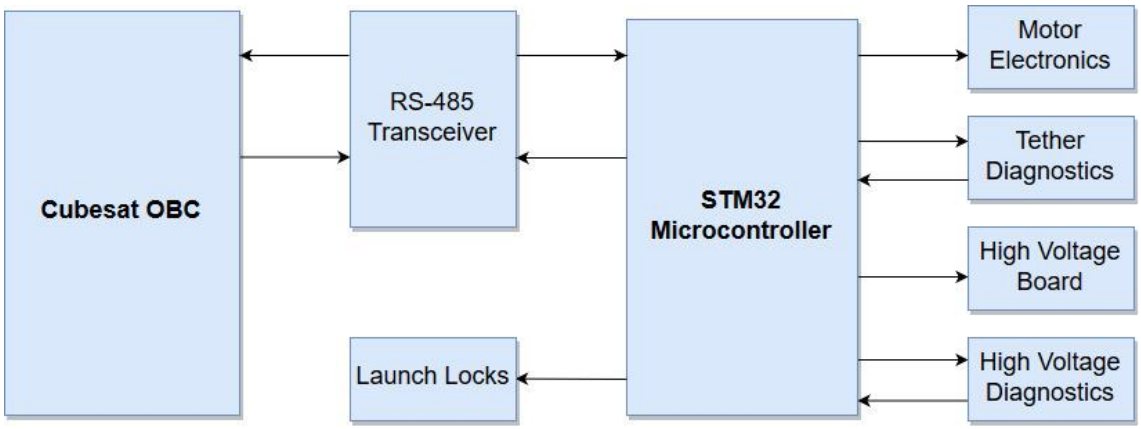

Figure 4. An overview of the plasma brake prototype. Two of the major differences between the electric sail and plasma brake is the requirement of an electron gun for the electric sail. Aside from that the electrical designs are almost identical.

Figure 4 shows the full system for the electric sail and plasma brake. It shows that the physical layer of communication between our system MCU and the cubesat OBC will be carried out by TIA-485 (Commonly referred to as RS-485) transceivers. RS-485, however, does not define any communication protocol or packet encapsulation for the system.

The figure 4 also includes the high voltage board subsystem, which is utilised for providing the large electric potential for the tethers, but will not be covered by this thesis. The high voltage diagnostics would simply consist of measuring tether voltage and current via ADCs. Measurements, unfortunately, were not possible during the time of writing this thesis.

The system will be used to drive and monitor a bipolar stepper motor with two phases, each phase rated for 1.8A with a full step equaling to 1.8 degrees. A stepper motor was chosen, as it is mechanically accurate with positioning and has no brushes that may fail during deployment, or worse, destroyed during launch vibrations.

The maximum speed and power of the motor can be described with the following equations:

$$\frac{Voltage}{2 * inductance * \text{maximum}\, current * steps\ per\ revolution} = Maximum\ speed \quad (1)$$

Using the rated current and voltage, the following value is acquired.

$$\frac{2V}{2*1.85*10^{-3}H*3.6A*400spr} = 0.375\ revolutions\ per\ second \quad (2)$$

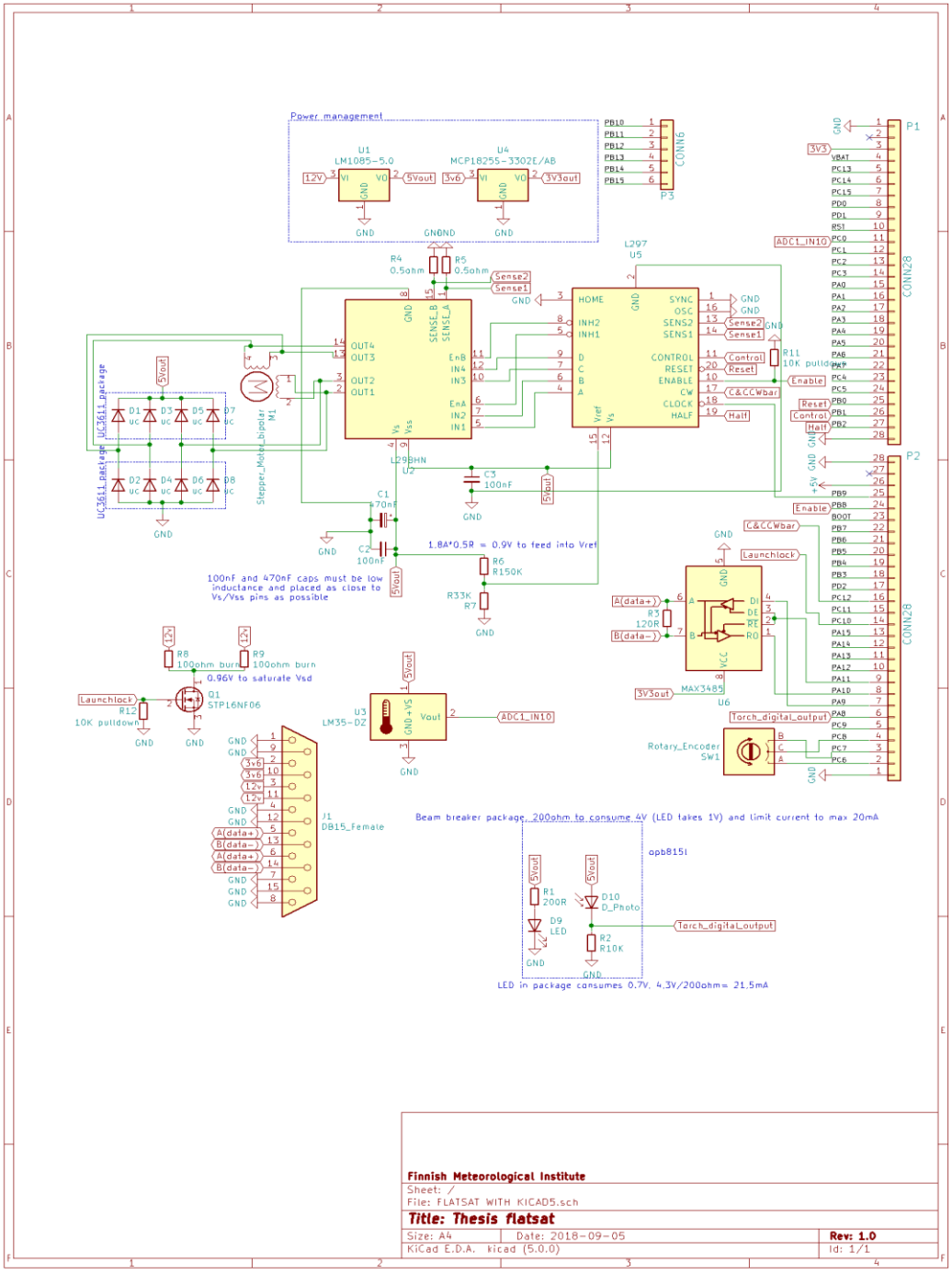

Figure 5. System Schematic.

Figure 5 depicts the schematic of the system. Several components are bordered into blue boxes as they either represent an IC package or subsystem. Much of the prototype is based around datasheet and application note designs, with a couple discrete components added to increase system stability and compatibility.

3.1 Systems

3.1.1 Microcontroller and Communication

The main microcontroller of choice for controlling the system is an STM32F1 MCU. This MCU is chosen as it has an extensive flight and space heritage, incredibly important when robustness and reliability are major concerns of a system. It is CMOS 32-bit microcontroller architecture developed by STMicroelectronics that is based upon the ARM Cortex-M3 core.

We will be implementing a value line model (STM32F100RBT6B) that is housed on a STM32VL discovery kit to ease prototyping. The key features of this model include 128KB Flash memory, max speed of 50MHz, 8KB RAM, on-board ST-LINK for code upload, user LEDs, USER and Reset push buttons and a system operation voltage of 3V [4]. It contains many five volt tolerant pins for TTL interfacing.

For this prototype, communication with the MCU is handled by USB to UART breakout board LC231X. Commands are sent via PC to the LC231X using YAT serial terminal program, with the first returned value being the command value sent. The communication protocol used is a simple ring buffer and transfer buffer for handling memory as provided by cubeMX code initialising software. The rest of the protocol is defined as half-duplex at 115,2Kbauds with one stop bit and no parity bit. This is a very simple protocol and suitable for in-house prototyping.

The schematic in figure 5 also depicts an EIA-485 transceiver. This transceiver was not tested due to lack of appropriate cables, equipment and no EIA-485 based protocol. It was still added to the PCB due to its simplicity, so that it may be tested later.

3.1.2 Motor Electronics

The main systems of the deployment system include the stepper motor, control electronics and the MCU. This system is primarily composed of the L298 and L297 stepper motor control and drive chip combination. These two components have existed since the 1980s and are still used today, primarily in automotive and industrial settings, but also personal projects as well. They are easy to implement and only require a few external components to function. The L297 is responsible for executing the complicated control signaling, while the L298 is a power management IC that delivers the high currents to the phases of the motor.

They are robust and reliable, but lack many of the recent innovations that are included in many modern chips. Features such as microstepping, or step error detection, which both exist on many modern chips, are not included. Some of these functions are still implementable using external components, and supposedly microstepping is possible using programming tricks.

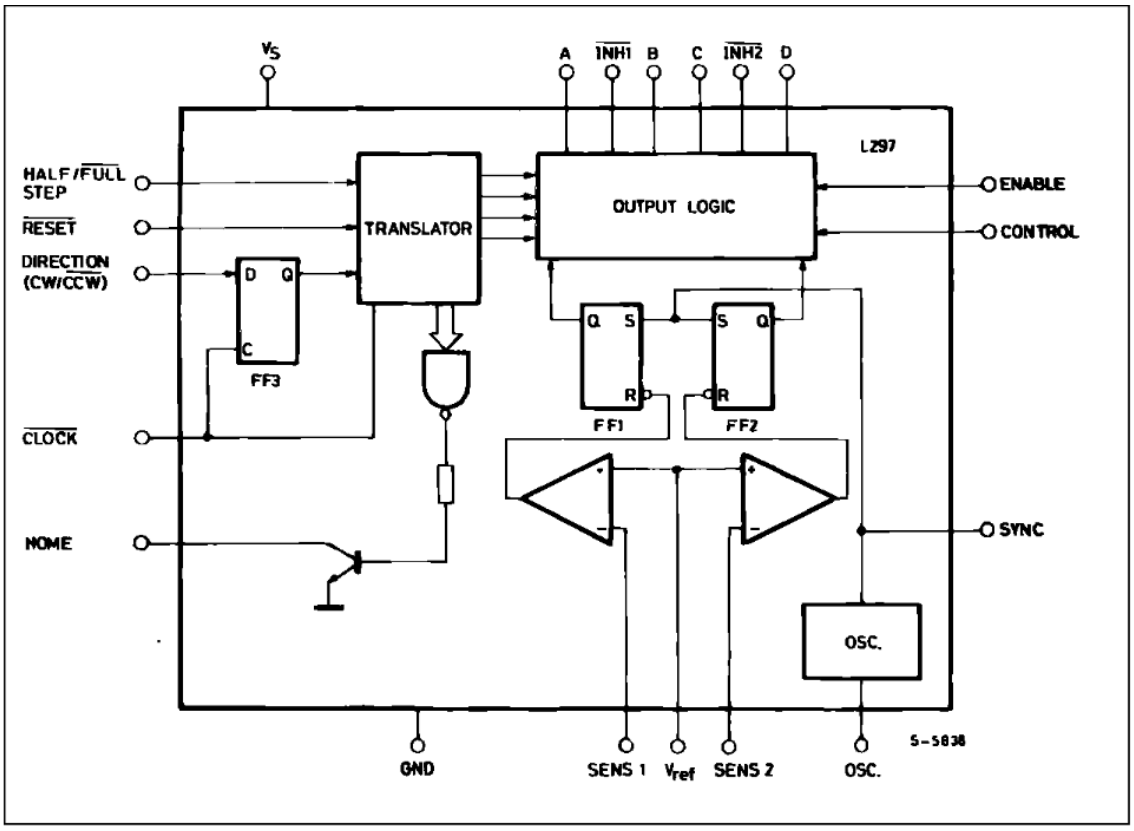

Figure 6. L297 circuit diagram. Reprinted from [5]

There are several external components vital for the proper operation of the motor deployment system. Smoothing capacitors are required to remove inductive ringing caused by the fast switching within the L298 and L297. In case of successful execution of microstepping, recirculation diodes were added to the system to allow for quick current changes within the motor windings. Due to the STM32 MCU tristating its pins on bootup/reset, a 10K pulldown resistor was added to the enable pin of the L297 to prevent the motor electronics from drawing unnecessary current due to booting or resetting the MCU. Figure 6 details some of the inner workings of this particular IC and the role that the sense resistors serve. The L298 will output its phase currents also through the current sense resistors, which is monitored by a comparator within the L297 and compared to a reference voltage. Once the sensed voltage reaches the same value as the reference, the L298 is then cut until the next control signal is received.

0.5ohm current sense resistors were chosen due to easy availability. Using this parameter and the 1.8A as specified by the motor, we can calculate the required voltage for L297's chopping circuit by using Ohm's Law.

$$0.5R * 1.8A = 0.9V \tag{3}$$

By using a voltage divider circuit from the 5V supply to pin 15 of the L297, we can deliver 0,9V. High values for the resistors are desirable as this will reduce power consumption.

$$0.9V = \frac{5V*33kR}{150kR+33kR} \tag{4}$$

Control will be handled directly by the MCU by pulsing the clock pin of L297 with a square wave, thus eliminating the need for the Sync and Oscillator pins of the L297. The unused pins may be tied to ground unless otherwise specified by the manufacturer. The home pin of L297 should output a 5V signal whenever the motor is switched to a predefined position. Due to failure to achieve its functionality during breadboard testing, it was omitted from the design, thus the pin is also tied directly to ground. It may still prove useful for discerning motor positioning in conjunction with an encoder, if the L297 makes it to the EQM.

3.2 Subsystems

3.2.1 Tether Diagnostics

For diagnostics, several parameters of the motor must be measurable. These parameters include rotary speed (revolutions per second) and motor temperature. Additionally a method to detect the tipmass status, is required.

The requirements of detecting the tipmass are rather simple, it is only necessary to check that it is still locked in place until mission execution. A slotted optical switch is a simple solution, using an infrared light emitting diode and an NPN silicon phototransistor integrated into a single package. In this prototype, the component is designated OPB815L. The light emitting diode only requires about 0.7V to turn on, so when operating on 5V it is necessary to burn off the excess 4.3V with an external resistor and keep the current low. By adding a 200ohm resistor, the following current value is calculated:

$$\frac{4.3V}{200ohm} = 21.5mA \tag{5}$$

A pulldown resistor to ground is added to the digital output signal from the package. This will ensure that the value will not float into an unwanted state, by pulling it logic low when the photodiode is not conducting. The output will be about 5V when logic high, so care must be taken to connect this to an input pin that is tolerant to 5V.

Measurements of motor position and speed is obtainable with a quadrature encoder. This is a package consisting of a light emitting diode and an array of phototransistor, along with filtering elements to produce a digital square wave at its outputs. For this prototype, an AEDB-9140 TTL quadrature encoder that does not require external components was chosen. Despite external components not being a requirement, pullup resistors from signal outputs to the 5V supply are recommended. The encoder is combined with a code-wheel and both are secured to the motor.

Quadrature encoders have typically two to three digital outputs, two of which create regular pulses that are 90 degrees out of phase, typically named channel A and channel B. This offset allows the direction of the rotation to be determined (unnecessary for this prototype).The additional channel I is used for measuring revolution.

A quadrature encoder can be realised to detect both the falling and rising edges in conjunction with a MCU. By using a timer and timer capture function on the STM32, we can create some basic code and formulas to detect rotary speed, how many revolutions have been made and position.

Finally, temperature of the motor coil windings must be measured. This is a slightly redundant feature for this prototype, as the FM stepper motor will have an embedded temperature sensor. Additionally, there is no need for higher accuracy than the 12-bit accuracy offered by the analog to digital converters in the STM32.

A simple and ready calibrated sensor such as LM35DZ should be sufficiently accurate. The device scales a linear output voltage of 10mV/Centigrade and is directly proportional to the temperature of the leads. This IC does not require external components or calibrations to function accurately. With some thermal adhesive, the temperature sensor can be fixed directly to the motor windings, after removing the stepper motor back-plate.

3.2.2 Launch Locks

As earlier mentioned, vibrations during launch are one of the largest hazards to be encountered by the payload. These vibrations can not only damage the soldering of the electronics, but also pose a mechanical risk to the tether reel and the tipmass (which must be situated on the surface of the satellite). Due to this, a simple locking system is required for ensuring that the reel and tipmass stay in place up until deployment. The locking solution used by most cubesat designers is rather simple, implementing mylar strings wrapped around resistors. When the locks are to be released, the resistors are burnt with a signal sent from the MCU.

A simple MOSFET used as a switch to conduct the 12V line through two 100ohm resistors in parallel will serve the role of launch locks for this prototype. The total resistance of these resistors will be:

$$\frac{100R+100R}{100R*100R} = 50R \tag{6}$$

The MOSFET in use is well suited for switching, designated P16NF06. Using this MOSFET the resistors will not see 12V when switched on, MOSFET consumes 1V internally to switch on. This will leave an 11V drop on the resistors, still sufficient. Following this, the current passing through the resistors according to Ohm's Law:

$$\frac{11V}{50R} = 0.22A \tag{7}$$

$$0.22A * 11V = 2.42W \tag{8}$$

The resistors should be chosen to be capable of withstanding the above calculated power dissipation and voltage drop, so that repeated tests may be carried out. As with the case on the L297 enable pin, a pulldown resistor is added to the gate pin of the MOSFET to ensure it remains off until the corresponding command is sent.

3.2.3 Power Management

For managing voltage requirements, two LDOs are required. These LDOs will be used to change a 12V supply to 5V and a 3.6V supply to 3.3V. Efficiency for this prototype is not necessary, so step-down converters will not be implemented to drop 12V to 5V.

LM1085IT-5.0/NOPB is a non-adjustable LDO that can take a wide range of input voltages. It has a dropout of 1.3V to function, so a minimum of 6.3V must be supplied in order to operate. For dropping 12V to 5V, the LDO will burn the excess 7V within its internal circuitry, this combined with a high amp draw of possibly up to a maximum of 3A on this prototype, will lead to significant heating and power consumption within the IC. This component is limited to a maximum current draw of 3A, to reduce risk of component or PCB failure.

$$7V * 3A = 21W \tag{9}$$

21W is the peak power dissipated by the LDO when the stepper motor is operated at its rated voltage. This is a very large problem as it only allows for short run times with the motor, before LM1085IT-5.0/NOPB will suffer catastrophic failure. However, the flexibility of LDOs allows them to be used over a wide voltage range. Most results of

this report were achieved with 6.3V supplied to the LDO, but without any mechanical load for the motor.

12V is one of the voltages given on FORESAIL-1 cubesat and this prototype uses FORESAIL-1s electrical specifications provided as a basis and for initial prototyping. It is far simpler to use LDOs rather than implementing step-down and step-up converters, which complicate design and expand the scope of this study considerably.

MCP1825S-3302E/AB was used for changing the other provided voltage of 3,6V to 3,3V. It is also nonadjustable and is current limited to a maximum of 500mA. The minimum dropout for this LDO is 210mV at 500mA. Use of an LDO to drop 3,6V to 3,3V is acceptable for the EQM and even the FM, as the energy loss is rather insignificant.

$$\frac{3{,}3V}{3{,}6V} = 0{,}916666\ldots \tag{10}$$

92% efficiency is within perfectly tolerable limits, especially as this LDO will only be drawing low currents. This degree of efficiency is close, near same, to what is achievable with a step-down converter, but without the added complexity.

4 Results

This section will cover the results and measurements made of the system. The tools involved were a digital oscilloscope and a digital multimeter. Most measurements presented will be snapshots taken from a digital oscilloscope. In most cases, the voltages in the system were analysed.

4.1 PCB and Design

The PCB had few design requirements for correct operation. The bypass capacitors were placed as close to the switching ICs as possible. This reduces any possible ringing that may incur due to undesired inductances in the PCB traces. Heatsinks were added to the components that dissipated the most power. Several peripheral devices were chosen to

be implemented externally from the PCB, notably the temperature sensor and the optical sensors.

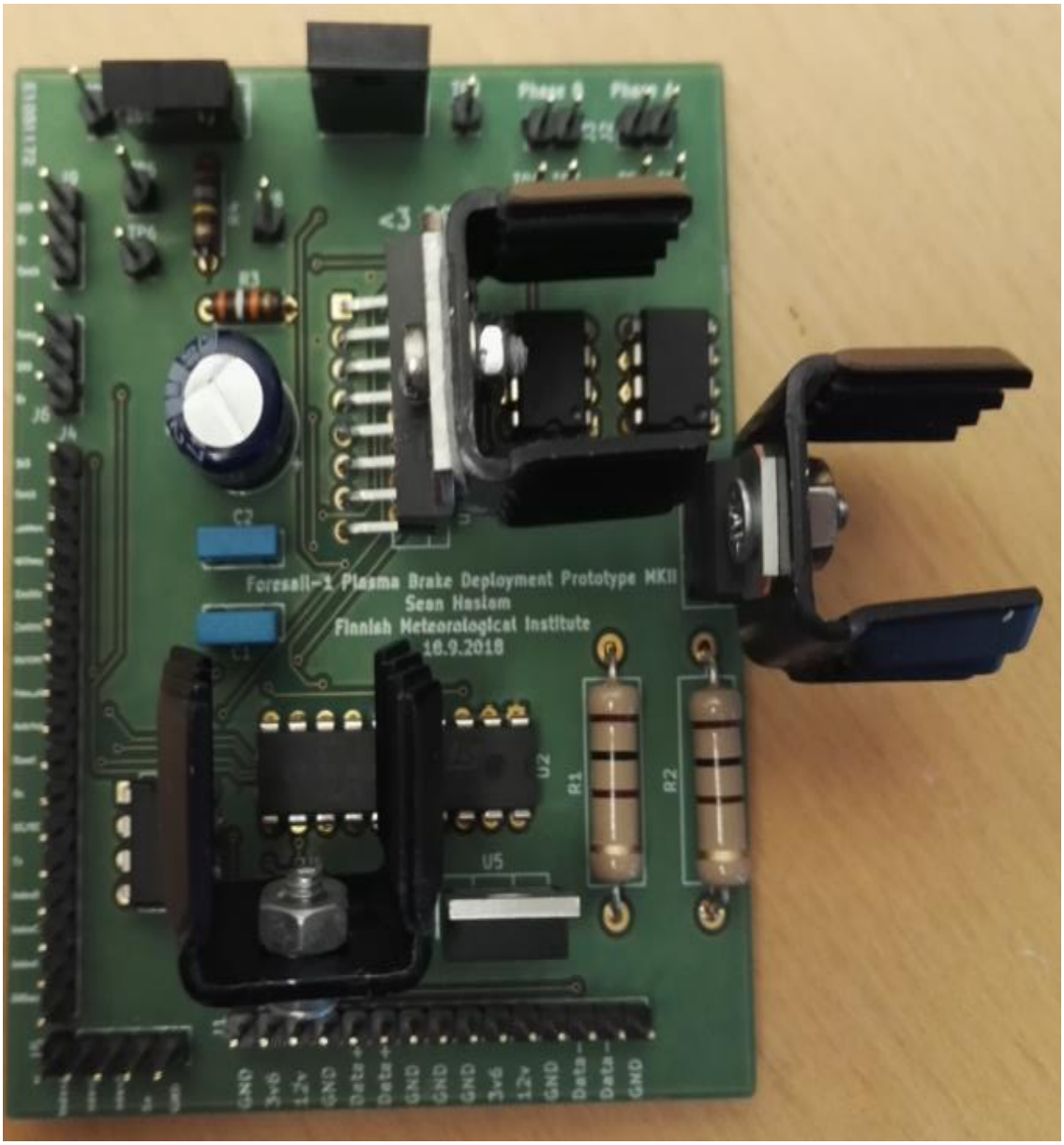

Figure 7. PCB prototype.

Above is the first fully finished prototype. It is printed on a two layer board, with the ground implemented onto the top layer. Components are completely soldered from the bottom layer, and consists entirely of through-hole and dual in-line packages. Several test points were added, so that various measurements can be easily attained. There is one test

point that is situated on the ground, used as a reference point for taking all other measurements. Test points for measuring the sense resistor voltages and the voltages over the voltage divider for L297s reference pin were added. Motor phases also have test points added on this PCB, however they proved ineffective for taking measurements due to nonlinearities in the L298 circuit.

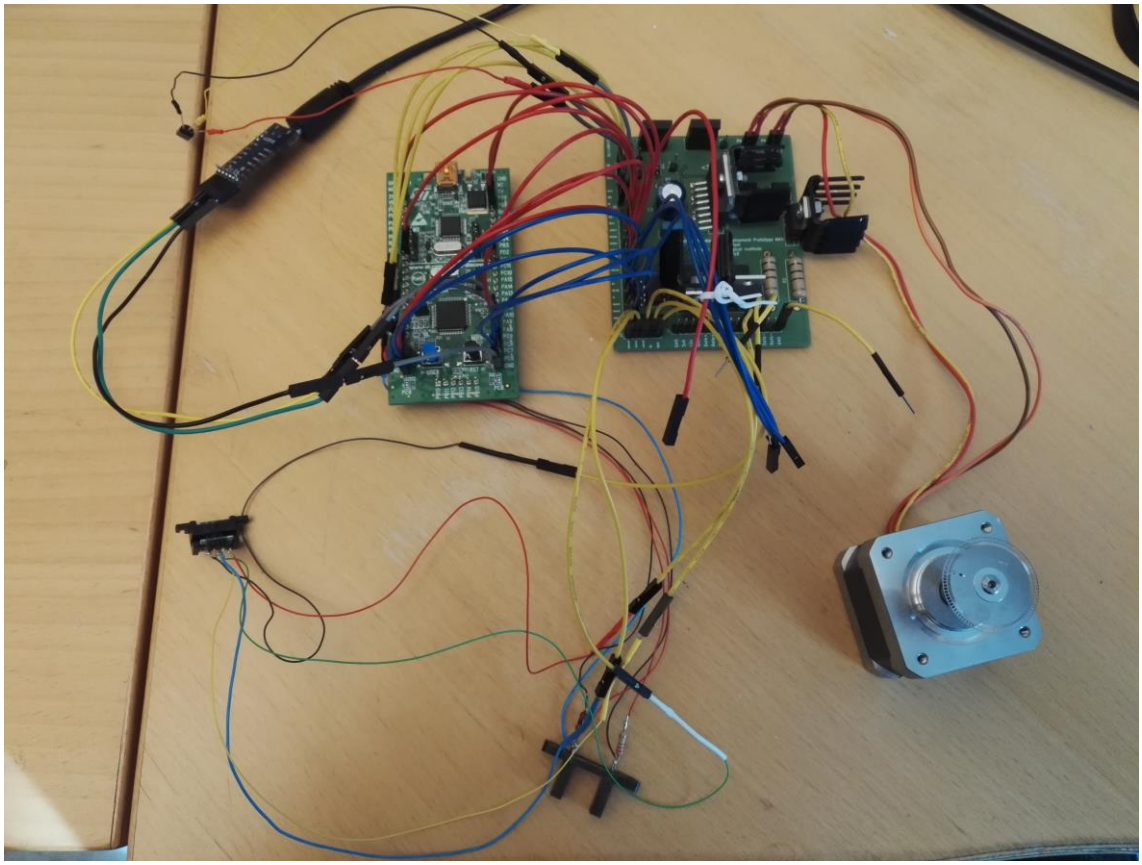

Figure 8. Full system.

Figure 8 shows the full system, including the motor and various other components that were impractical to solder onto the PCB, such as the temperature sensor and the optical switches. Connections to other devices and peripherals, such as the MCU, LC231X and quadrature encoder were made using pin headers and jumper wires.

4.2 Motor Driving

By far, the most important results are for motor driving, as it is the main function of this prototype. It is necessary to mention that the following measurements were made without

a load for the motor. Torque and other similar requirements were unknown at the time of this study. Torque is directly proportional to motor winding current, so power consumption may vary with a dummy load.

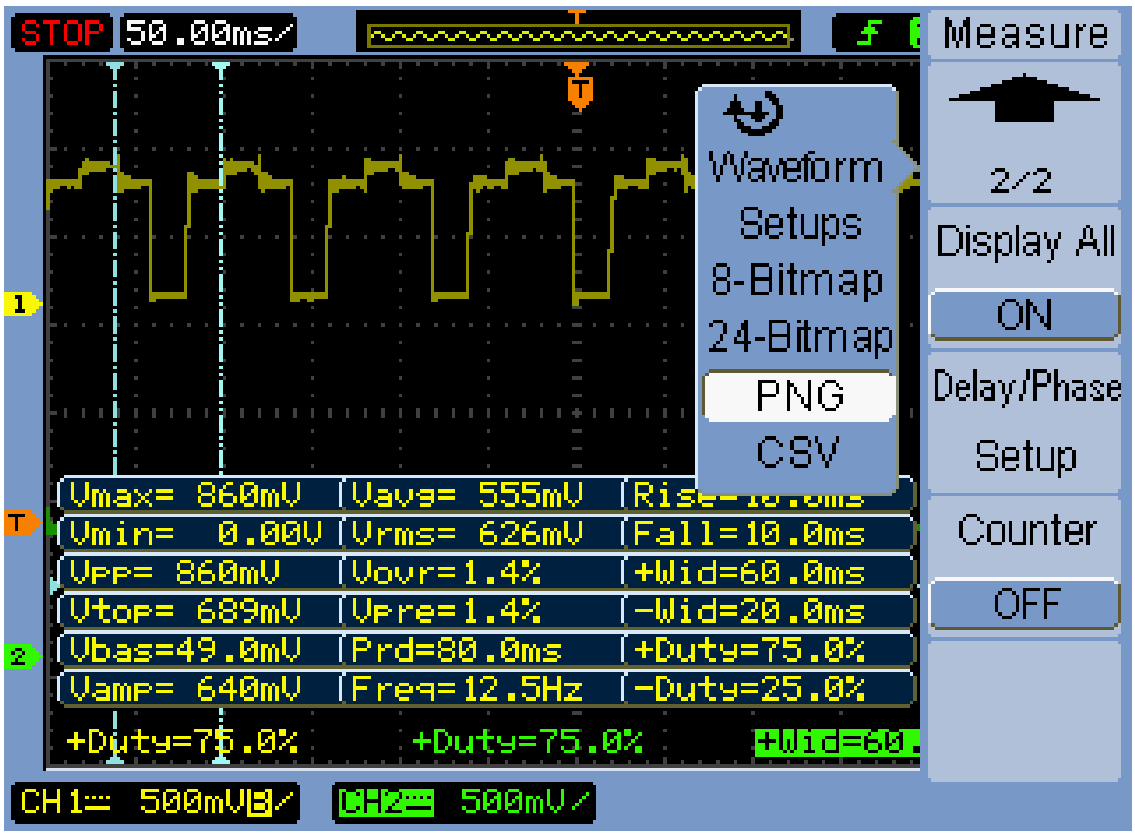

Figure 9. Phase A.

In figure 9, we can see the motor winding output for phase A, as measured from the current sense resistor. The measurement was made in half-step operation. Within each phase, there are three distinct states visible in a period. Peak voltage reaches 860mV, but settles close to 840mV during the peak state. This is close enough to the intended 900mV supplied to the Voltage reference pin of the L297. The duty cycle per phase remains at about 75%. The x-axis cursors can be ignored, they do not contribute to the measurements.

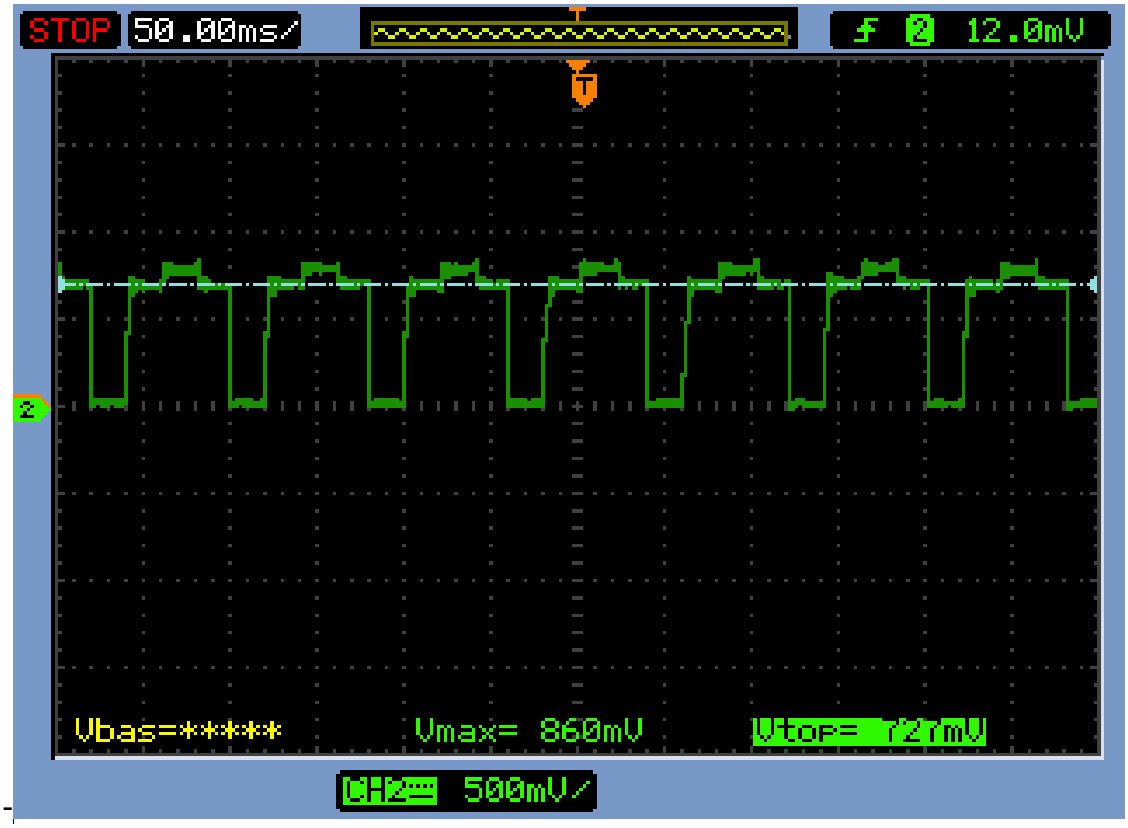

Figure 10. Phase B.

Figure 10 shows a similar waveform with mostly the same values for phase B, but offset by 90 degrees. The y-axis cursor shows from where Vtop is measured. Values are close to the same as in phase A, but the noise introduced into both phases causes some small variations.

4.3 Tether Diagnostics

4.3.1 Motor Status

The results for motor status were less than satisfactory. Problems with the temperature sensor at ambient made any results at higher temperatures inconclusive. There were also mechanical issues with connecting the quadrature encoder to the code-wheel on the stepper motor.

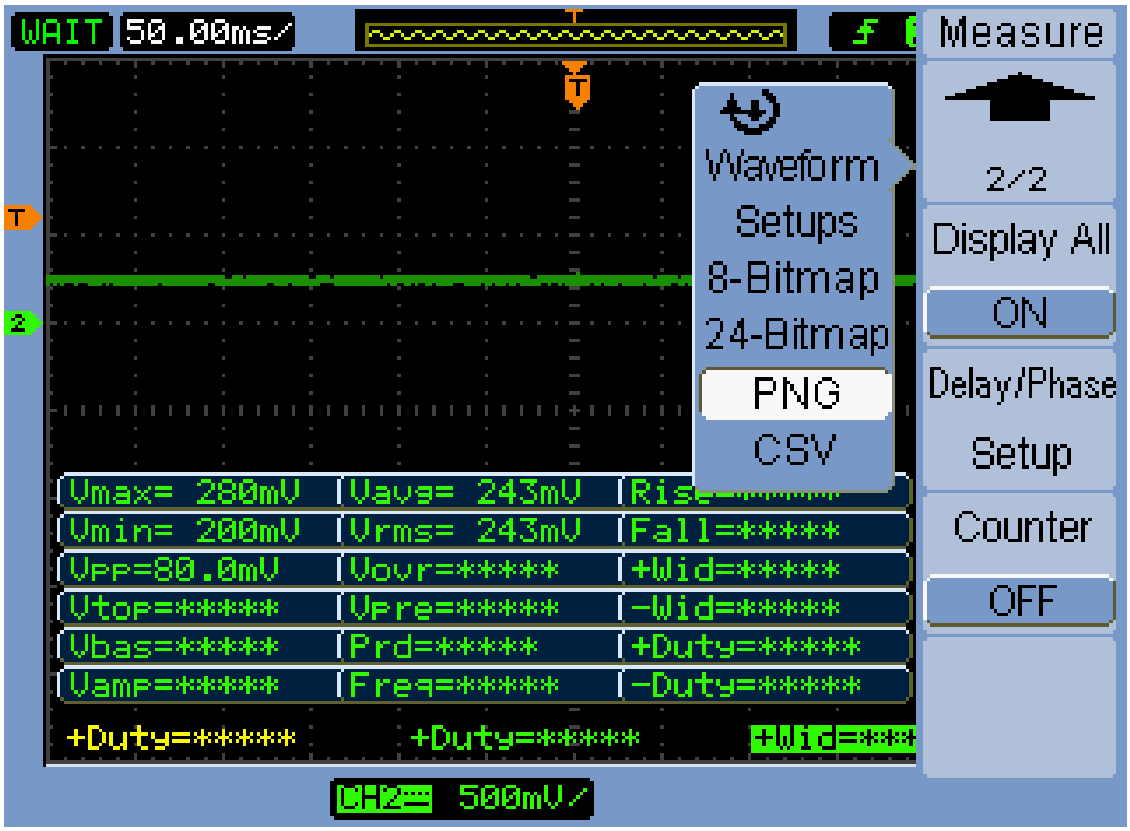

Figure 11. Temperature measurement.

Figure 11 shows the value of the LM35DZ output when tested at 21 degrees (ambient), measured with an oscilloscope. This measurement clearly shows that the calibration or implementation of the IC is incorrect. The output is fairly noisy, jumping between 200mV and 280mV

$$\frac{243mV}{10mV/C} = 24.3\ degrees \tag{11}$$

This value differs significantly from the values returned by the analog to digital converters embedded in the STM32.

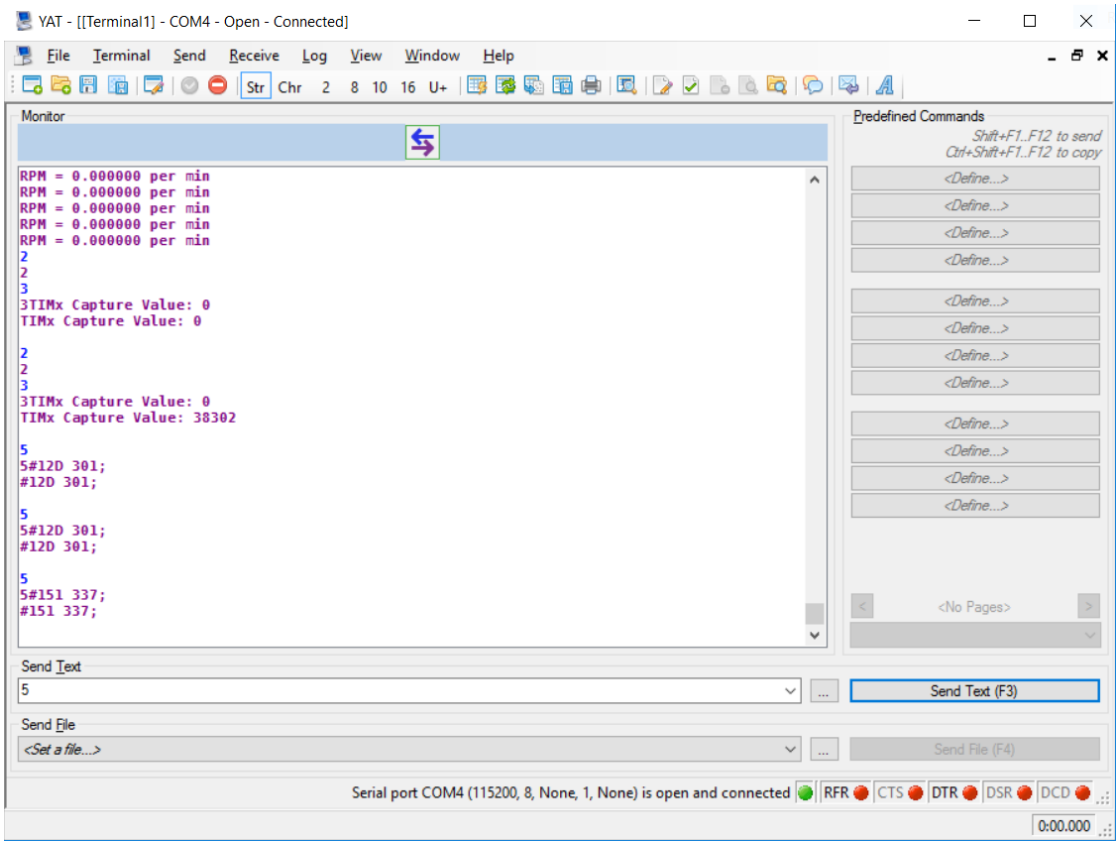

Figure 12.

In figure 12, analog to digital converter measurements are shown as received by the serial terminal, after sending command “5” marked in blue. The first value is a hexadecimal value limited to 3 characters and the second is simply an integer value. A value of 301 is first received, then after some light manipulation of the IC, a value of 337. These readings can be converted to corresponding voltage values with the following equation:

$$\frac{Received\ Terminal\ Value * STM32\ operating\ voltage}{4095} = Voltage \quad (12)$$

$$\frac{301*3}{4095} = 220mV \quad (13)$$

$$\frac{337*3}{4095} = 247mV \quad (14)$$

220mV corresponds to 22 degrees and 247mV to 24.7 degrees. The first value is significantly closer to the 21 degree ambient, but still outside of the promised accuracy of the IC.

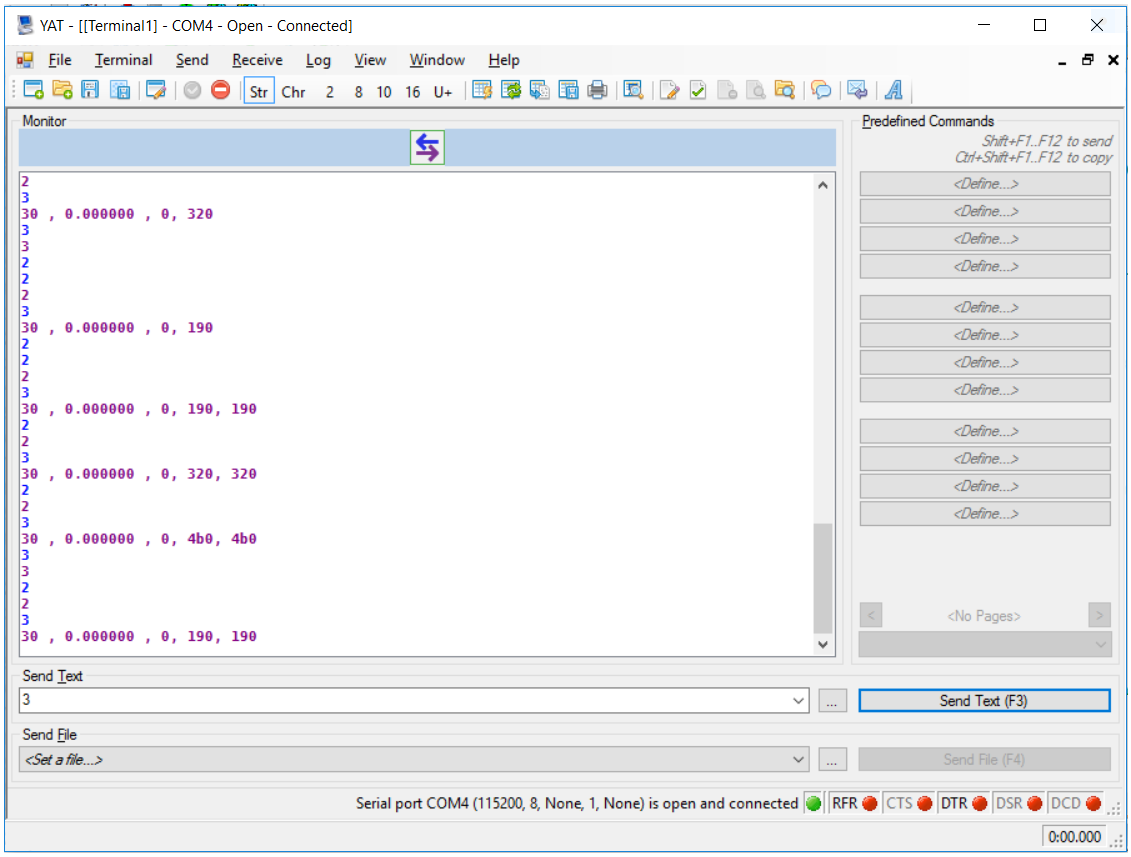

Figure 13. Encoder values.

Figure 13 displays the values returned by the STM32 to the personal computer terminal. It shows the failed results of the quadrature encoder in purple, and the commands sent in blue. The first value was meant to express total degrees moved, the second value to express revolutions per minute, third value to express how many error steps occurred, fourth value expresses the amount of correct steps and finally the last value is supposed to list how many times the “for loop” that is responsible for pulsing the L297 clock pin has run. Testing was setup so that the last value would be a known value, as the motor was set to spin a set amount of revolutions for measurement purposes as dictated by code. This last value is supposed to show up as 400 on the terminal, which is clearly not the case.

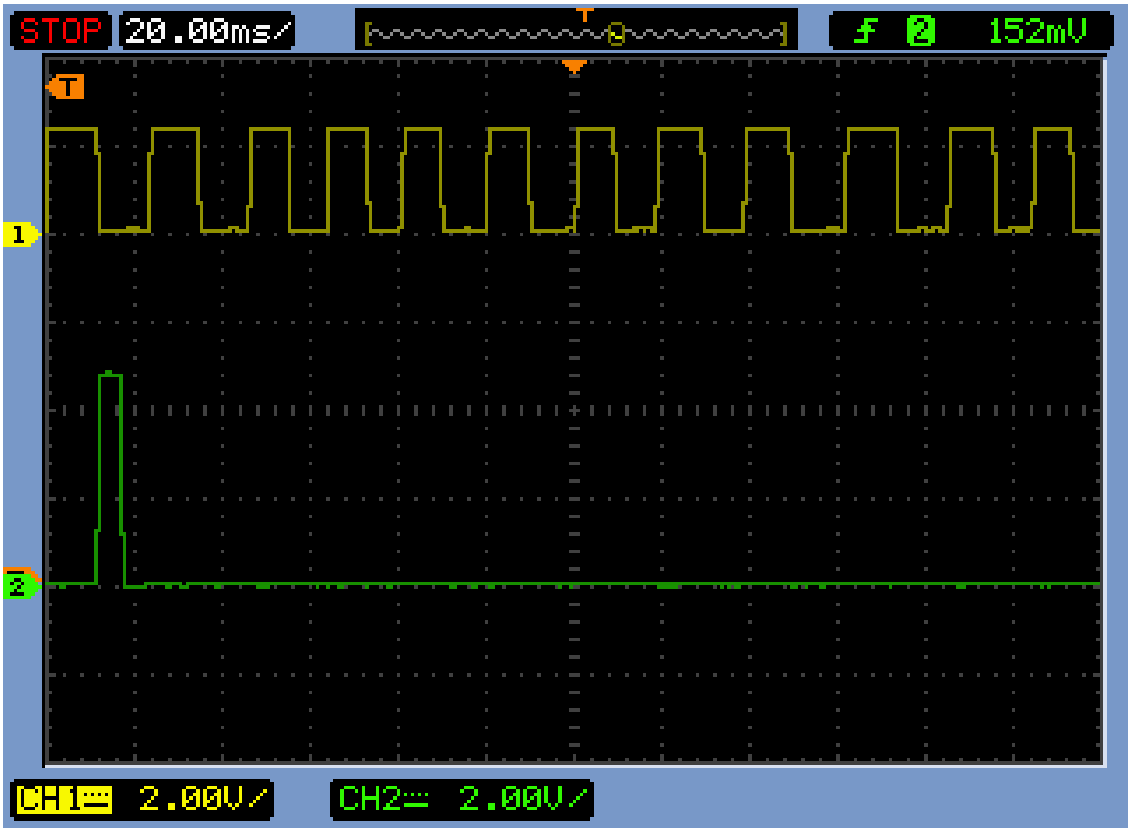

Figure 14. Oscilloscope measurement of encoder.

Figure 14 contains oscilloscope measurements of the system, with the encoder poorly attached to the code-wheel and motor. Only channel A and channel I are measured, Channel I represents one revolution per pulse, while 400 pulses of channel A equals to one revolution. Channel I has a digital voltage level of close to 5V, however channel A only shows slightly over 2V. This signal level is not adequate to be detected as a digital signal by a CMOS device, which requires an accurate value closer to 3V at the very minimum to be recognised as a digital signal.

Due to time constraints, the quadrature encoder was abandoned in favour of using another slotted optical switch package, which can measure the rotations and rotation speed accurately enough for this prototype. Figure 12 in fact shows a measurement with this setup using a timer set to count in milliseconds. This timer counts one falling edge per revolution for sake of simplicity and the timer is started upon starting the motor. According to the terminal a rotation occurred in 38302 milliseconds. By dividing 60000 by this value, 1.56 revolutions per minute is achieved. During that particular measurement, the L297 clock pin was pulsed with a square wave with a period of 100ms and duty cycle of

50%, the L297 will send the next stage control signals to the L298 on the falling edge of this square wave. While in half step mode, in theory, the motor requires 400 steps to complete one revolution, if step errors or such were not to occur. Following this it should take approximately 40 seconds to complete one revolution, if 1 half step were to occur every 100ms, but as the code is run line by line, small errors are expected to accumulate. Additionally, the width of the opaque material fixed to the motor shaft was enough to return logic state of “0” within the optical switch for several half steps. The timer measurements of figure 12 are by no means accurate, but it is a good starting point to refine this subsystem further.

4.3.2 Tipmass Status

This subsection will conclude the motor status and tether diagnostics with measurements of the slotted optical switch. It was manually blocked with an opaque object to simulate the tipmass. The main concern of measurement is the voltage, as the STM32 requires a digital signal level of 3 volts to read digital inputs properly.

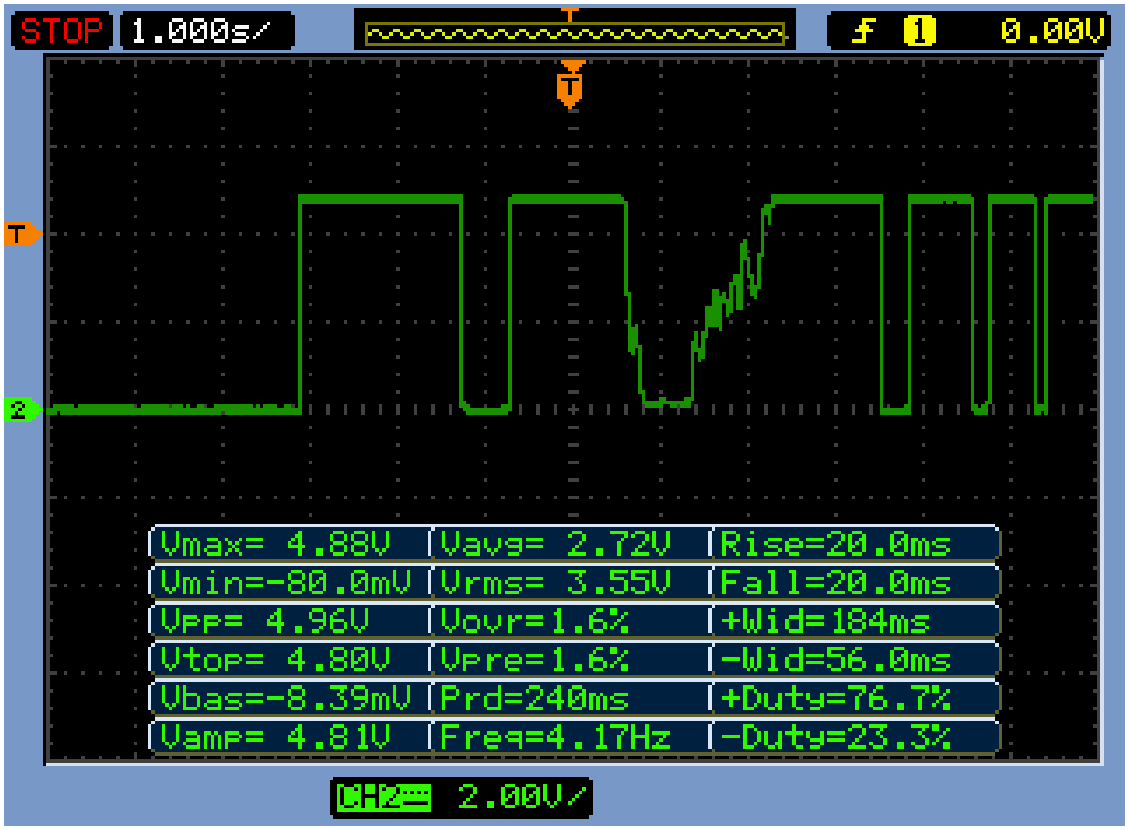

Figure 15. OPB15L measurement.

Figure 15 indicates the results acquired from the optical switch device. While the beam is collimated, the collimation is not perfect, as can be seen from the second dip and third rising edge. Slow blocking of the infrared light shows that the device may be susceptible to some degree of misalignment error. An output of 4.9V is adequate to be read as a digital signal by the MCU.

4.4 Launch Locks

The main concern of measurement for the launch locks is the current. A digital multimeter in series with the launch lock resistors shows how much current is drawn when the MOSFET is switched on. This is the only subsystem of the deployment system that requires 12V.

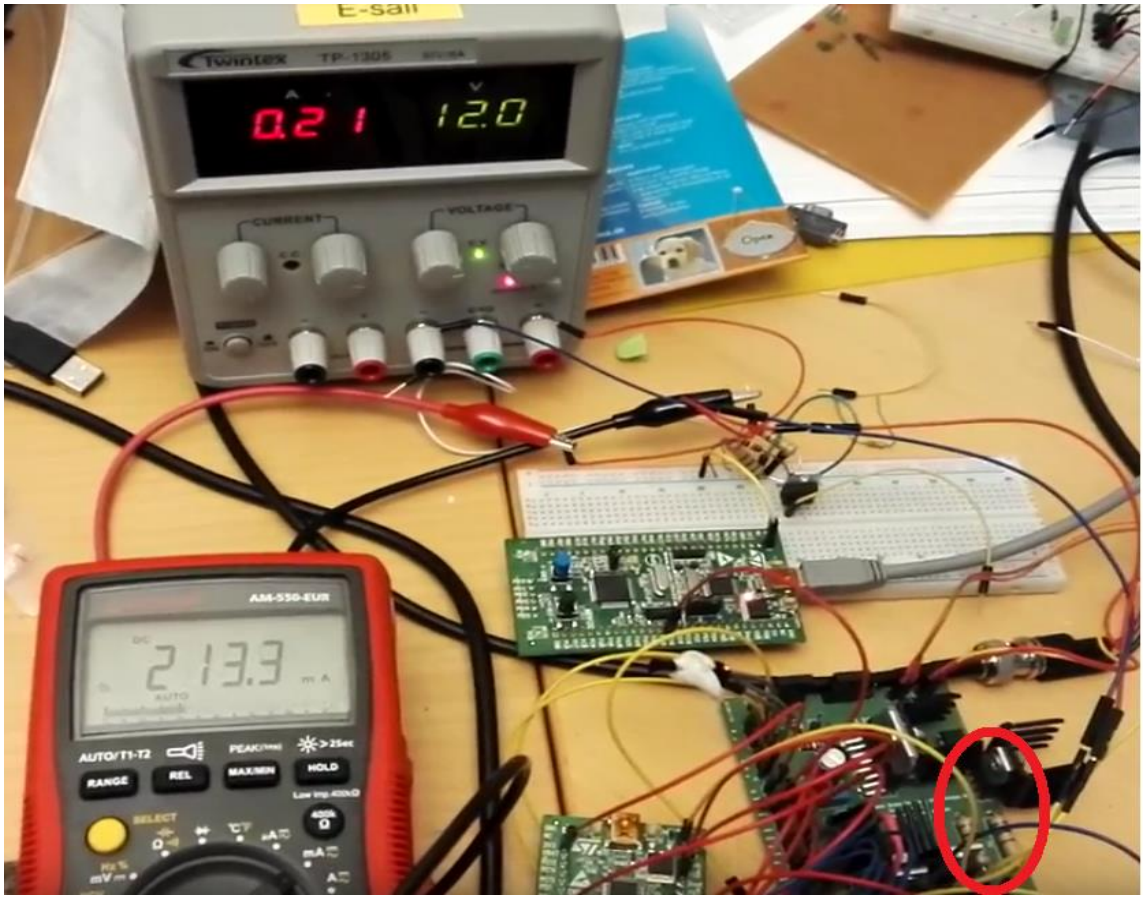

Figure 16. Launch lock's current consumption.

As figure 16 shows, the result of current draw for the launch locks follows the calculations closely. Losses are probably due resistor value accuracy and possible additional minor resistance added by cables and jumper wires.

4.5 Power Management

It is good practice to have some method available for measuring the output voltage and currents of any voltage regulators. Testing of the LDOs may reveal causes of other measurement errors and transient effects.

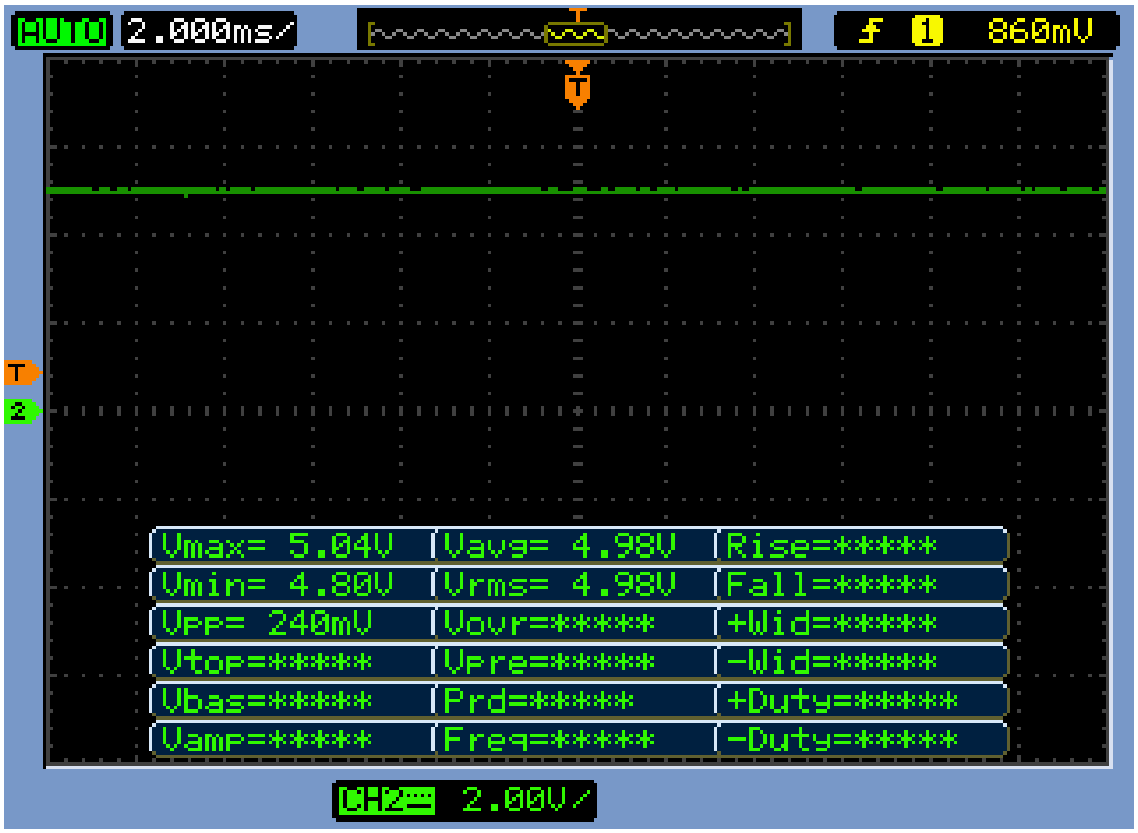

Figure 17. Voltage divider for L297 Voltage reference.

According to figure 17, the total voltage outputted from the LDO LM1085IT-5.0/NOPB is very close to 5V, but shows slight deviation. However, this deviation is too small to cause any issues with the instruments or motor. Sadly, there is no way to measure the LDO MCP1825S-3302E/AB output. During initial designs, it was never considered a require-

ment to measure the outputs of both LDOs. The voltage divider for the L297 was necessary for the circuit and by pure serendipity, makes an ideal test circuit for the LDO LM1085IT-5.0/NOPB. There was a failure to add any test circuitry for LDO MCP1825S-3302E/AB, but everything powered from it worked correctly regardless.

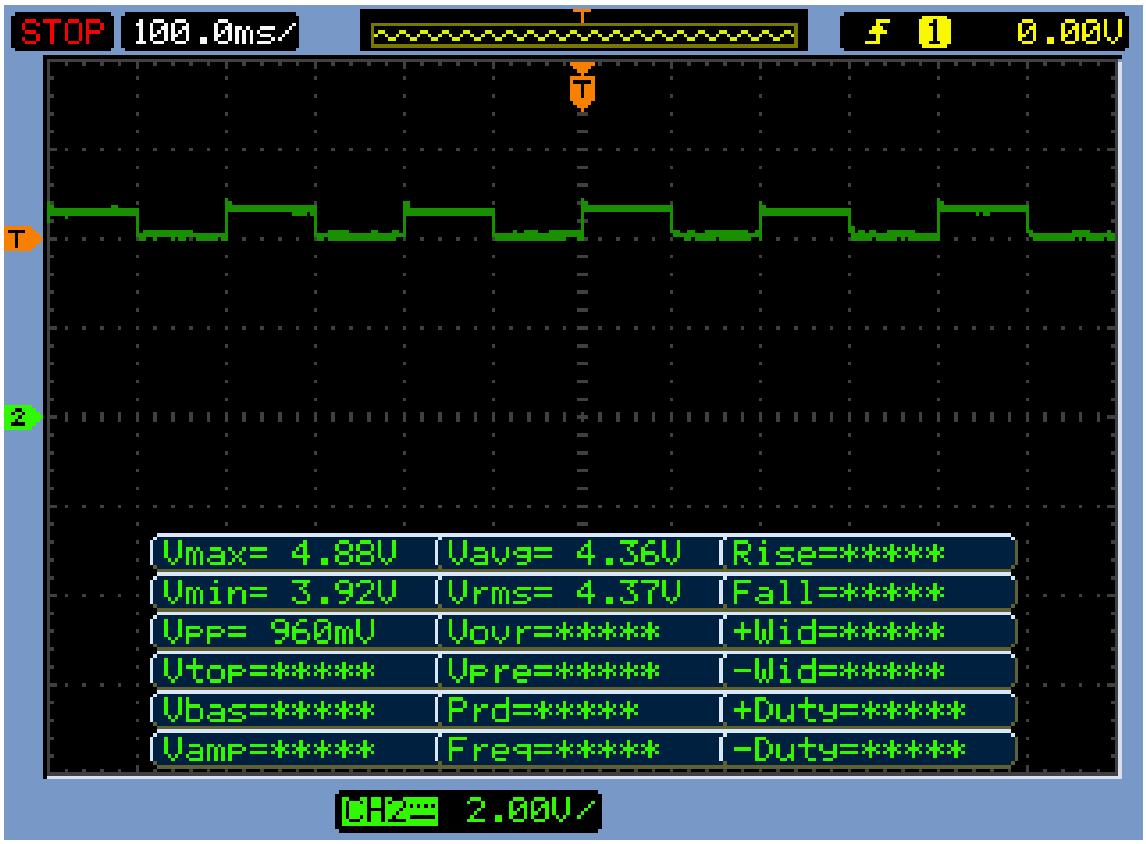

Figure 18. Voltage divider during motor driving.

Above in figure 18, is the total voltage drop over the voltage divider network for L297. This measurement was made during motor drive. Value drifts considerably from supplied 5V during motor operation, while the switching is indirectly visible in the waveform. Since the voltage remains below 5V and varies by almost an entire volt, the value provided as a reference will also be wrong, thus the motor is driven by a voltage lower than what it is intended.

5 Conclusions

The prototype was successful in relation to the project needs. The main requirement of this project was to deliver a MCU controlled motor that can be used to reel out short

pieces of tether in a laboratory environment, which was accomplished. Problems arising from the quadrature encoder can be easily sorted out by substituting it with another slotted optical switch and simply fixing an opaque material to the stepper motor shaft. This may not allow accurate measuring of the position, in the event of error steps, but it eases the process of prototyping the diagnostic subsystems for later improvements. The shaft piece may then be further customized for the purposes of this project, to accurately deduce position and determining error step frequency. Future models will also further investigate motor driving with various voltages, to implement the best balance of power efficiency and torque for the motor.

Moreover, difficulties and inaccuracies with the temperature sensor are of little consequence. Later deployment system models will use a flight-grade motor with an embedded temperature sensor. For this reason, understanding the functionality of the MCU analog to digital converters was more important than the temperature measurements. Additionally, the MCU analog to digital converters will be used to measure tether voltage and current when in high voltage operation mode after deployment.

5.1 Future

5.1.1 Protocol

As UART nor EIA-485 define a true protocol, one must be developed to ensure proper handling and reading of data. Such a packet encapsulation would be based off the EIA-485 standard. This protocol must also implement cyclic redundancy code to prevent and fix data corruption.

5.1.2 Flatsat to EQM to FM

Preliminary satellite prototypes are typically referred to as flatsats, and are the initial stage of prototyping a satellite payload. They are to be interfaced with a prototype of the OBC, so that a complete prototype of the satellite may be tested. The model that follows the flatsat is referred to as an engineering qualification model. This model, depending on mission requirements, may implement flight-graded components as required. Most of the functionality is already decided and successfully prototyped at this stage. It, however,

still remains partially comprised of commercial off-the-shelf components. Finally, a FM is produced. This is the actual device to be launched into space, fully functional with flight-grade components and materials. It must still undergo several serious tests, vibration testing as an example. It must also pass a rigorous solder inspection and be entirely clean of any contaminates.

One of the main changes to future models will be the implementation of a sophisticated power management subsystem with nonlinear converters. A cubesat's power is provided by lithium-ion batteries that are charged using solar panels. Often it is up to the payload teams to design the various regulated and current limited voltages lines that they need directly from these batteries. Besides power management, several other alterations are expected to be made to the next prototype. In addition to the motor, there shall be a sophisticated launch lock system with its own embedded diagnostics.

This concludes the study of the prototype. Overall, the electric sail and plasma brake are very promising technologies for use in space travel. The simulations of these technologies provides compelling proof of concept to necessitate an investigation into the practicality of these propulsion methods. Needless to say, the key concern of these technologies is in the deployment. Such a task has not been accomplished in space to this date, making it an ambitious endeavour to undertake.

References

[1] The CubeSat Program, Cal Poly SLO (2014). *CubeSat Design Specification Rev.13*. Available at: https://static1.squarespace.com/static/5418c831e4b0fa4ecac1bacd/t/56e9b62337013b6c063a655a/1458157095454/cds_rev13_final2.pdf

[2] P. Janhunen. (2008). Electric Sail – *A New Propulsion Method Which May Enable Fast Missions to the Outer Solar System.* Available at: http://electric-sailing.fi/Aosta2007.pdf.

[3] P. Janhunen, P. Toivanen and J. Envall. (2017) *Electrostatic Tether Plasma Brake.* Available at: http://electric-sailing.fi/papers/BB15-LSIversion-with-execsum.pdf

[4] STMicroelectronics. (2014). *STM32VLdiscovery.* Available at: https://www.st.com/resource/en/data_brief/stm32vldiscovery.pdf

[5] STMicroelectronics. (2001). *L297 datasheet.* Available at: https://www.st.com/resource/en/datasheet/l297.pdf